ELSEVIER

Biophysical Chemistry 116 (2005) 213 – 218

Biophysical Chemistry

http://www.elsevier.com/locate/biophyschem

C-terminus of a long α-neurotoxin is highly mobile when bound to the nicotinic acetylcholine receptor: A time-resolved fluorescence anisotropy approach

David A. Johnson*

Division of Biomedical Sciences, University of California, Riverside, Riverside, CA 92521-0121, United States

Received 8 February 2005; accepted 17 March 2005
Available online 13 May 2005

Abstract

To better understand how α-neurotoxins interact with the acetylcholine receptor, four fluorescein isothiocyanate derivatives of the *siamemsis* α-cobratoxin were prepared (conjugated to the ε-amino group in Lys^{23}, Lys^{35}, Lys^{49}, or Lys^{69}) and the time-resolved fluorescence anisotropy of each conjugate was measured free in solution and bound to the *Torpedo* acetylcholine receptor. All the conjugated reporter groups displayed a high and comparable level of mobility free in solution. When receptor bound, on the other hand, significant differences in the conformational dynamics of the reporter groups were observed with the C-terminal Lys^{69} derivative displaying by far the greatest mobility strongly suggesting that the C-terminal domain of the bound neurotoxin is highly mobile and does not participate in the toxin–nAChR binding surface. Additionally, this study demonstrates the utility of time-resolved fluorescence anisotropy to characterize the interaction of heteroproteins.

Keywords: α-Cobratoxin; Nicotinic acetylcholine receptor; Conformational dynamics; Time-resolved fluorescence anisotropy

1. Introduction

α-Neurotoxins have played crucial role in the pharmacological and structural characterization of muscle-type and α7 neuronal nicotinic acetylcholine receptors (nAChR). In the absence of an X-ray crystal structure, a variety of physical approaches have been utilized for more than three decades to delineate the structural basis for the interaction of α-neurotoxins with the nAChR. These include chemical cross-linking [1–3], computer enhanced electron microscopy [4], fluorescence resonance energy transfer [5,6], NMR spectroscopy [7], single-site [8], and pairwise [9] mutational analyses and molecular simulation [10].

To contribute further to our understanding of the interaction of α-neurotoxins with the nAChR and to assess the utility of time-resolved fluorescence anisotropy (TRFA) to probe heteroprotein interactions, we prepared a small library of α-cobratoxins, a 'long' α-neurotoxin, that were selectively conjugated with fluorescein-5-isothiocyanate (FITC) and measured the mobility of the reporter group in each conjugate free in solution and receptor bound. Specifically, the TRFA of FITC conjugated to the ε-amino group in Lys^{23}, Lys^{35}, and Lys^{49}, and Lys^{69} was measured both free and bound to the *Torpedo* nAChR. Free in solution, each site of conjugation displayed an almost equal and high level of mobility. Receptor bound, clear differences between the sites of conjugation were observed with the C-terminal Lys^{69} conjugate displaying the greatest mobility. The results strongly suggest that the C-terminal tail is not part of the binding surface being highly mobile in the bound state and argues against conclusions from recent computational docking simulation [10] and a free-solution NMR study [7].

* Tel.: +1 951 827 3831; fax: +1 951 827 5504.
E-mail address: david.johnson@ucr.edu.

0301-4622/$ - see front matter © 2005 Elsevier B.V. All rights reserved.
doi:10.1016/j.bpc.2005.03.010

2. Experimental procedures

2.1. Materials

α-Cobratoxin was isolated following the method of Karlsson et al. [11] from *Naja naja siamensis* venom (Miami Serpentarium, Salt Lake City, UT). *Torpedo californica* electric rays were obtained from Marinus Inc. (Long Beach, CA). Dansyltrimethyl-ammonium perchlorate was acquired from Pierce Chemical Co. (Rockford, IL). Fluorescein-5-isothiocyanate (Isomer I) was obtained from Molecular Probes, Inc. (Eugene, OR). The procedure for labeling α-cobratoxin with FITC and isolating derivatives with the FITC bonded to the ε-amino groups of Lys^{23}, Lys^{35}, Lys^{49}, or Lys^{69} of the α-cobratoxin is described elsewhere [12]. All other reagents were at least reagent grade.

2.2. Isolation of the membrane-associated nAChR

nAChR-associated membrane fragments were prepared from the *T. californica* electric organs following previously described procedures [13]. The specific activity of the receptor preparation was 4.4 nmol of suberyldicholine binding sites/mg of total protein, determined as described elsewhere [14].

2.3. Sample preparation

For the measurements of the emission decay properties of the free conjugates, native α-cobratoxin (5 μM) was incubated with nAChR-enriched membrane fragments (0.5 μM in suberyldicholine binding sites) in a buffer containing 100 mM NaCl, 10 mM $NaPO_4$, and 0.1% triton X-100, pH 7.4 for 30 min prior to the addition of the conjugated toxin (0.3 μM). The native α-cobratoxin was not included when the decay properties of the nAChR-bound conjugates were measured. This sample preparation protocol equalized and minimized the turbidity ($A < 0.05$) of all the samples. Also, given that native toxin binds with 10–100 fold higher affinity than the conjugates [12], little or no conjugate was specifically bound to the nAChR in the presence of native toxin.

2.4. Time-resolved fluorescence anisotropy

Emission anisotropy was determined by time-correlated single photon-counting with an HORIBA Jobin Yvon IBH Ltd. (Glasgow, U.K.) 480-nm NanoLED™ flash lamp run at 1 MHz, an HORIBA Jobin Yvon IBH Ltd. model TBX-04 photon detector, and two rotatable Polaroid HNPB dichroic film polarizers—one placed in the excitation beam path and one in front of the photon detector. The vertically, $I_{\|}(t)$, and orthogonally, $I_{\perp}(t)$, polarized emission components were collected while samples were excited with vertically polarized light. Excitation and emission bands were selected with an Oriel 500-nm short-pass interference (catalog no. 59876) and a Corning 3–68 cut-on filter, respectively. Typically, 2×10^4 peak counts were collected (in 1–2 min) when the emission polarizer was vertically oriented. The orthogonal emission decay profile was generated over the same time interval used to generate the vertical emission decay profile. Samples were held at 22 °C. To minimize convolution artifacts, flash lamp profiles were recorded by removing the emission filter and monitoring light scatter from a suspension of latex beads. The data analysis software corrected the wavelength-dependent temporal dispersion of the photoelectrons by the photon detector. The polarization bias (G) of the detection instrumentation was determined by measuring the integrated photon counts/6×10^6 lamp flashes while the samples were excited with orthogonally polarized light and the emission was monitored with a polarizer oriented in the vertical and orthogonal directions ($G = 1.028$).

The emission anisotropy decay was analyzed with the impulse reconvolution method implemented in the DAS6™ software package from HORIBA Jobin Yvon IBH Ltd. (Glasgow, U.K.) described elsewhere [15]. Briefly and simply, this approach splits the analysis into two steps—analysis of the total emission decay, $S(t)$, followed by analysis of the vertical/perpendicular difference emission decay, $D(t)$. $S(t)$, free of anisotropy effects, is given by the expression

$$S(t) = I_{\|}(t) + G \cdot I_{\perp}(t) \tag{1}$$

and was analyzed as a biexponential function. $D(t)$, which includes both fluorescence and anisotropy parameters, is given by the expression

$$D(t) = I_{\|}(t) - G \cdot I_{\perp}(t). \tag{2}$$

$D(t)$ is deconvolved with the results from the *S(t)* analysis as a constraint yielding

$$r(t) = r_{\infty} + r_o f_{xb} \exp(-t/\phi_{fast}) + r_o(1 - f_{xb}) \exp(-t/\phi_{slow}). \tag{3}$$

Here, r_{∞} is the amplitude of the experimental anisotropy at infinite time, r_o is the amplitude of the anisotropy at time zero, f_{xb} is the fraction of the anisotropy decay associated with the fast decay processes, and ϕ is the rotational correlation time of the anisotropy decay. The subscripts 'fast' and 'slow' denote the observable fast and slow decay processes, respectively. A nonassociative model was assumed, implying that the emission relaxation times are common to all the rotational correlation times. Goodness of fit was evaluated from the values of the reduced Ψ_r^2 and by visual inspection of the weighted-residual plots.

A technical note: The older approach of sequential fitting the sum and difference curves [15] instead of the newer simultaneous fitting of the vertical and horizontal decay curves [16] was used. Our experience is that both

approaches work and no comparison has been published favoring one over the other. For time-domain data, the commercial sum–difference software more rapidly fits and plots the data than the noncommercial globals program; consequently, the sum–difference approach was utilized for the work described here.

3. Results

3.1. Purity of the FITC–toxin derivatives

The conjugates studied were at least 97% pure based upon the observation that only a single fluorescence spot was detected for each conjugate following analytical isoelectric focusing and illumination with a mineral lamp. Additionally, as we previously reported, each toxin binds with high affinity to the *Torpedo* nAChR, K_d's range between 0.2 nM and 3.2 nM [13]. Moreover, neither the conjugation nor nAChR binding greatly affected the emission maxima, which ranged between 517 nm and 520 nm for the free conjugates and between 519 nm and 522 nm for the nAChR-bound conjugates [12].

3.2. Emission decay

The initial step of the anisotropy decay analysis involved least-squares re-convolution fits to a biexponential decay expression of the total fluorescence decay records. For brevity, only the quantum-yield weighted fluorescence lifetimes are summarized in Table 1 and an example of the total fluorescence decay (sum) of Lys^{23} conjugate is illustrated in Fig. 1. The quantum-yield weighted fluorescence lifetimes ranged between 2.2 ns and 3.6 ns when the toxins were free in solution and between 2.7 ns and 3.4 ns when nAChR-bound. Please note that we previously reported observing only a single emission lifetime for each conjugate using a less stable and longer duration hydrogen-arc flash lamp (1.0 ns versus 3.2 ns) [6].

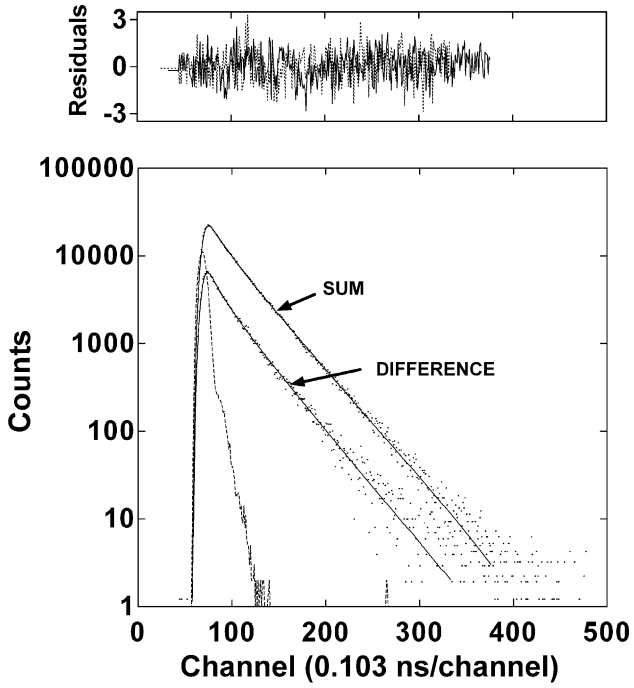

Fig. 1. Sum and difference decays of FITC–toxin conjugated at Lys^{23}. Lower panel: Smooth line through each decay were generated with best fit parameters of a biexponential expression (Eq. (3)). Dashed inverted U-shaped curve represents the time course of the flash-lamp profile. Upper panel: Sum (dashed line) and difference (solid) residuals for both fits.

The relative changes in lifetimes paralleled what was previously reported for the binding-dependent changes in steady-state emission; however, the magnitudes of these changes were generally less when lifetimes were measured (Table 1). For example, the steady-state emission of the Lys^{23} conjugate increased 96% upon nAChR binding while the quantum-weighted fluorescence lifetimes increased only 23% (comparison of results in Table 1 with Table 2 in Ref. [12]. This suggests differences in binding-dependent static and dynamic quenching. We assumed that these changes in static and dynamic quenching would not affect the anisotropy analysis. Consistent with this assumption are

Table 1
Time-resolved anisotropy decay parameters and quantum-yield weighted fluorescence lifetimes of the site-specifically labeled α-cobratoxins free and bound to the nAChR

Toxin conjugate	Condition	r_o[a]	r_∞[b]	f_{xb}[c]	ϕ_{fast} (ns)	ϕ_{slow} (ns)	ψ_r^{2d}[d]	$<\tau>$[e] (ns)	I_b/I_f[f]
FITC–Lys^{23}–Toxin	Free	0.30±0.04	–	0.42±0.09	0.6±0.4	4.4±1.5	1.2±0.1	2.2±0.1	
	Bound	0.29±0.01	0.21±0.01	0.29±0.02	3.0±0.3	∞	1.0±0.2	2.7±0.1	1.96
FITC–Lys^{35}–Toxin	Free	0.29±0.01	–	0.38±0.15	1.0±0.4	5.5±3.2	1.0±0.1	3.4±0.1	
	Bound	0.33±0.04	0.20±0.03	0.39±0.03	2.7±0.1	∞	1.0±0.1	3.1±0.1	0.61
FITC–Lys^{49}–Toxin	Free	0.28±0.02	–	0.48±0.03	0.7±0.1	5.7±0.5	1.0±0.1	3.0±0.1	
	Bound	0.34±0.03	0.23±0.03	0.31±0.02	2.7±0.4	∞	1.0±0.2	3.1±0.1	0.94
FITC–Lys^{69}–Toxin	Free	0.27±0.01	–	0.30±0.06	0.9±0.2	4.6±1.7	1.0±0.1	3.6±0.1	
	Bound	0.26±0.02	0.14±0.02	0.47±0.03	2.2±0.2	∞	0.9±0.1	3.3±0.1	0.74

[a] Time-zero ($t=0$) anisotropy.
[b] Residual anisotropy ($t=\infty$).
[c] Fractional anisotropy decay associated with the fast decay processes.
[d] Reduced ψ_r^2 of the anisotropy decay analysis.
[e] Quantun-yield weighted fluorescence lifetime in which $<\tau>=\sum a_i\tau_i$ and where τ_i is the ith lifetime and the sum of the preexponential terms $\sum a_i=1$.
[f] Fractional change in steady-state emission associated with nAChR binding (values from Ref. [12]).

the facts that neither negative preexponential intensity fitting parameters (data not shown) nor inverted U-shaped anisotropy decay profiles were observed with any of the toxin conjugates.

3.3. Anisotropy decay of free FITC–α-cobratoxins

In situations where the reporter group is largely unhindered at the end of a tether on the surface of a relatively structured globular protein (>40 kDa), the fs–ps local tether-arm, the very low nanosecond α-carbonyl backbone, and the low nanosecond whole-body depolarization processes can usually be resolved from one another [17]. The tether-arm fluctuations are observed as a time-zero anisotropy (r_o) value that is lower than the fundamental (immobile) anisotropy. The local backbone fluctuations and whole-body rotational diffusion are represented by the fast and slow correlation times of a biexponential decay expression. With this in mind, free in solution, all the FITC–toxins display very similar anisotropy decay parameters (Table 1). With all the fitting parameters floating except r_∞ (fixed at zero), the anisotropy decay profiles (Fig. 2A) were well fit to a biexponential function (Eq. (3)). The slow rotational correlation times, ϕ_{slow}, ranged between 4.4 ns and 5.7 ns, which are very close to the harmonic mean correlation time (5.2 ns) predicted from the X-ray coordinates of the α-cobratoxin (PDB code: 2ctx.pdb) with the HYDROPRO.EXE program that utilizes bead-model methodologies to calculate hydrodynamic properties [18]. The fractional amplitudes, f_{xb}, and fast rotational correlation times, ϕ_{fast}, of the various labeled toxins overlapped each other and ranged between 0.30–0.42 and 0.6–1.0 ns, respectively.

Because the calculated values of the fast correlation times were close to the value of free fluorescein (~0.3 ns; data not shown), it suggested that the torsional tether-arm fluctuations might not be resolved from the backbone fluctuations around each conjugated residue. Consequently, the data were refit to a biexponential function (Eq. (3)) with r_o fixed at the value of the fundamental anisotropy of fluorescein (0.35) and again r_∞ fixed at zero. This modified fitting protocol yielded Ψ_r^2 values and weighted-residual plots that were very comparable to that observed with r_o floating (data not shown). Additionally, while the ϕ_{slow} values were unaffected by changing the fitting protocol, the values of the f_{xb} terms were increased and the ϕ_{fast} values were decreased somewhat ranging between 0.47–0.57 and 0.3–0.5 ns, respectively. The effect of modifying the fitting protocol on the fitting parameters clearly indicates a greater uncertainty in the f_{xb} and ϕ_{fast} values than suggested by the error terms in Table 1. This is probably due to the cross correlation of the fitting parameters. With this said, even with higher uncertainty in the f_{xb} and ϕ_{fast} values, the results still indicate significant and comparable level of torsional and/or segmental mobility for each site of conjugation of the FITC–toxins free in solution.

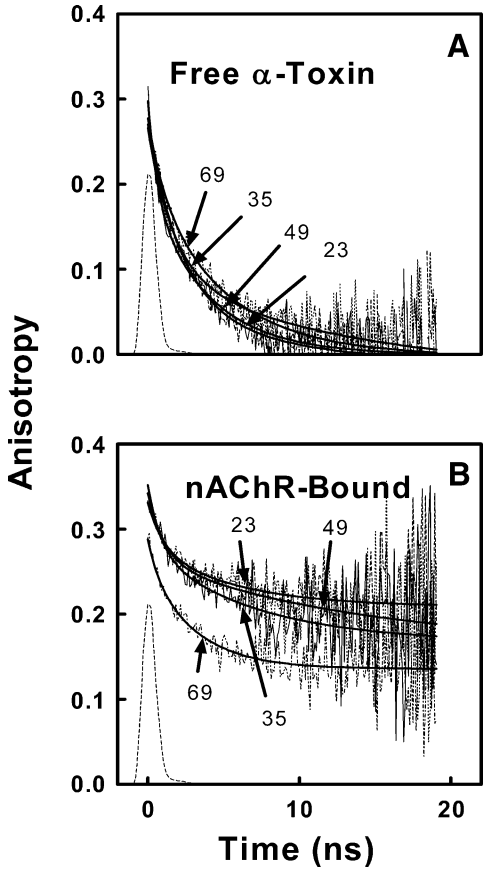

Fig. 2. Time-resolved anisotropy decay of free (upper panel) and nAChR-bound (lower panel) FITC–toxins. The smooth line through each decay was generated with best fit parameters (Table 1) for either biexponential (Eq. (3)) with $r_\infty=0$ (upper panel) or monoexponential with $r_\infty>0$ (lower panel) nonassociative decay model. Dashed inverted U-shaped curve represents the time course of the flash-lamp profile.

3.4. Anisotropy decay of nAChR-bound FITC–α-cobratoxins

Receptor binding affected the anisotropy decay in primarily three ways:

First, the anisotropy decay profiles shifted from biexponential functions decaying to zero ($r_\infty=0$) to monoexponential functions with residual anisotropy values ($r_\infty>0$) (Fig. 2B; Table 1). The appearance of residual anisotropy most likely results from the dramatic decrease in the whole-body rotational diffusion of the ~8 kDa α-cobratoxins upon binding the 250+ kDa nAChR.

Second, the experimental r_o values of the Lys^{35} and Lys^{45} conjugates increased and approached the fundamental (immobile) anisotropy value of fluorescein (0.35) suggesting increased hindrance of the tether-arm moments (Table 1). This suggests at least a partial sandwiching of the reporter groups between the toxin and the receptor that occurs, which will lead to a merging of the rates of tether-arm torsional motions with local backbone fluctuations around Lys^{35} and Lys^{49}. The r_o values of the Lys^{23} and Lys^{69} conjugates, on the other hand, were basically

unchanged by nAChR binding (Table 1) strongly suggesting no binding-dependent hindrance of tether-arm movement and thus no sandwiching of reporter group between toxin and receptor.

Finally, the fast rotational correlation times of all the conjugates increased upon binding (Table 1). While the interpretation of the changes in the rate of the fast depolarization processes for the Lys^{35} and Lys^{49} conjugates is complicated by the apparent merging of rates of tether-arm and backbone movements, the combined averaged tether-arm and backbone motions of the Lys^{35} and Lys^{49} conjugates indicate substantial range of motions. This is seen by assuming strict diffusion-in-cone and using the formulations of Kinosita et al. [19] which yield estimated conical semiangles of 32° for the Lys^{35} conjugate and 28° for the Lys^{49} conjugate when nAChR-bound.

For the for the Lys^{23} and Lys^{69} conjugates, there was no apparent merging of rates of tether-arm and backbone motions. The ϕ_{fast} values increased from 0.6 ns to 3.0 ns for the Lys^{23} conjugate and from 0.9 ns to 2.2 ns for the Lys^{69} conjugate (Table 1). This suggests some binding-dependent stabilization of backbone movements around the Lys^{23} and Lys^{69} residues. If stabilization is occurring, it is much greater around Lys^{23} than Lys^{69}, because the f_{xb} value of the Lys^{23} conjugate decreased from 0.42 ns to 0.29 ns, while that of the Lys^{69} conjugate increased from 0.30 to 0.47 ns (Table 1). Assuming this as strict diffusion-in-cone, the semiangle of the conical motions for Lys^{23} decreased from 34° to 27° and for Lys^{69} increased from 28° to 36° upon binding. Given that Lys^{69} is part of the C-terminal tail (residues 63–71) and is not stabilized by disulfide bonds like most of the toxin residues, the above results indicate that the C-terminus is unconstrained in the receptor-bound state and is therefore not a significant part of the toxin-receptor binding surface.

As a technical note, the nAChR-bound data were also fit with the r_o values fixed at 0.35, and although Ψ_r^2 values were comparable to that observed with r_o floating, the weighted-residual plots were not randomly distributed indicating poorer fits (data not shown). Consequently, only the results of the r_o-floating protocol are reported here.

4. Discussion

Here, we report that the C-terminus of a 'long' α-neurotoxin, α-cobratoxin, is highly mobile while bound to the *Torpedo* nAChR using a combination of site-specific labeling and time-resolved fluorescence anisotropy. This strongly suggests that the C-terminus of the toxin does not play a significant role in the toxin–nAChR binding surface. Arguing against this conclusion are the findings of a recent computational docking study of α-cobratoxin binding to the α7 nAChR [10] and a free-solution NMR study of a 1:1 complex of α-bungarotoxin and a 18-mer fragment of the α subunit of the *Torpedo* nAChR [7]. The computation docking analysis utilized the static crystal structure of the toxin and a static homology model of the α7 nAChR based on the X-ray crystal structure of snail acetylcholine binding protein to ascertain the toxin–receptor binding surfaces. At best, this approach yields approximate ligand–target models of the interacting surfaces. With regard to the free-solution NMR approach, the concentration of the toxin-peptide complex was 1.5–2.0 mM. At this concentration and with an unconstrained peptide, the binding time of weakly interacting moieties is greatly enhanced giving the impression that these interactions are significant at physiologically relevant concentrations. These studies thus represent equivocal support for involvement of the C-terminus of 'long' α-neurotoxins in their interaction with the nAChR.

Consistent with our conclusion is the fact that FITC conjugation only decreases the affinity of the Lys^{69} conjugate toward the nAChR by a factor of 10 while the conjugation of Lys^{23}, Lys^{35}, and Lys^{49} decreases the affinity by factors that ranged between 105 and 160 [13]. Moreover, there is no evidence that the extended C-terminal tail of virtually all 'long' α-neurotoxins increases the binding energy. Both 'long' and 'short' α-neurotoxins bind with about equal affinity to the *Torpedo* nAChR ($5.7–8.2 \times 10^{-10}$ M) [20].

Beyond the narrow focus of this work, this study demonstrates the utility of time-resolved fluorescence anisotropy to analyze the interaction of heteroproteins.

Acknowledgements

I wish to thank Lanise Ja Tekelhaimanot for collecting the anisotropy data and to recognize the financial support from National Science Foundation Grant IBN-9515330.

References

[1] V.N. Damle, M. McLaughlin, A. Karlin, Bromoacetylcholine as an affinity label of the acetylcholine receptor from *Torpedo californica*, Biochem. Biophys. Res. Commun. 84 (1978) 845–851.
[2] A. Karlin, Molecular biophysics: going round in receptor circles, Nature 329 (1978) 286–287.
[3] A. Sobel, T. Heidmann, J. Hofler, J.-P. Changeux, Distinct protein components from Torpedo marmorata membranes carry the acetylcholine receptor site and the binding site for local anesthetics and histrionicotoxin, Proc. Natl. Acad. Sci. U. S. A. 75 (1979) 510–514.
[4] H.P. Zingsheim, F.J. Barrantes, J. Frank, W. Hanicke, D.C. Neugebauer, Direct structural localization of two toxin-recognition sites on an ACh receptor protein, Nature 299 (1982) 81–84.
[5] D.A. Johnson, J. Voet, P. Taylor, Fluorescence energy transfer between α-toxins bound to the acetylcholine receptors, J. Biol. Chem. 259 (1984) 5717–5725.
[6] D.A. Johnson, R. Cushman, R. Malekzadeh, Orientation of cobra α-toxin on the nicotinic acetylcholine receptor: fluorescence studies, J. Biol. Chem. 265 (1990) 7360–7368.
[7] H. Zeng, E. Hawrot, NMR-based binding screen and structural analysis of the complex formed between α-cobratoxin and an 18-mer cognate peptide derived from the α1 subunit of the nicotinic

acetylcholine receptor from *Torpedo californica*, J. Biol. Chem. 277 (2002) 37439–37445.
[8] E.J. Ackermann, E.T. Ang, J.R. Kanter, I. Tsigelny, P. Taylor, Identification of pairwise interactions in the α-neurotoxin-nicotinic acetylcholine receptor complex through double mutant cycles, J. Biol. Chem. 273 (1998) 10958–10964.
[9] S. Malany, H. Osaka, S.M. Sine, P. Taylor, Orientation of α-neurotoxin at the subunit interfaces of the nicotinic acetylcholine receptor, Biochemistry 39 (2000) 15388–15398.
[10] C. Fruchart-Gaillard, B. Gilquin, S. Antil-Delbeke, N. Le Novere, T. Tamiya, P.-J. Corringer, J.-P. Changeux, A. Menez, Experimentally based model of a complex between a snake toxin and the alpha 7 nicotinic receptor, Proc. Natl. Acad. Sci. U. S. A. 99 (2002) 3216–3221.
[11] E. Karlsson, H. Arnberg, D. Eaker, Isolation of the principal neurotoxins of two *Naja naja* subspecies, Eur. J. Biochem. 21 (1971) 1–16.
[12] D.A. Johnson, R. Cushman, Purification and characterization of four mono-fluorescein cobra-α-toxin derivatives, J. Biol. Chem. 263 (1988) 2802–2807.
[13] D.A. Johnson, J. Yguerabide, Solute accessibility to N^{ε}-fluorescein isothiocyanate-lysine-23 cobra α-toxin bound to the acetylcholine receptor. A consideration of the effect of rotational diffusion and orientation constraints on fluorescence quenching, Biophys. J. 48 (1985) 949–955.
[14] C.F. Valenzuela, J.A. Kerr, D.A. Johnson, Quinacrine binds to the lipid–protein interface of the *Torpedo* acetylcholine receptor: a fluorescence study, J. Biol. Chem. 267 (1992) 8238–8244.
[15] D.J.S. Birch, R.E. Imhof, in: J.R. Lakowicz (Ed.), Time-Domain Fluorescence Spectroscopy Using Time-Correlated Single-Photon Counting, Topics in Fluorescence Spectroscopy: Techniques, vol. 1, Plenum, New York, 1991, p. 1.
[16] J.M. Beechem, E. Gratton, Fluorescence spectroscopy data analysis environment a second generation global analysis program, in: Joseph Lakowicz (Ed.), Time-Resolved Laser Spectroscopy in Biochemistry, Proc. of SPIE, vol. 909, 1988, pp. 70–81.
[17] M. Gangal, S. Cox, J. Lew, T. Clifford, S.M. Garrod, M. Aschbaher, S.S. Taylor, D.A. Johnson, D.A. Backbone, Flexibility of five sites on the catalytic subunit of cAMP-dependent protein kinase in the open and closed conformations, Biochemistry 37 (1998) 13728–13735.
[18] J. García de la Torre, M.L. Huertas, B. Carrasco, Calculation of hydrodynamic properties of globular proteins from their atomic-level structure, Biophys. J. 78 (2000) 719–730.
[19] K. Kinosita Jr., A. Ikegami, S. Kawato, On the wobbling-in-cone analysis of fluorescence anisotropy decay, Biophys. J. 37 (1982) 461–464.
[20] R. Chicheportiche, J.P. Vincent, C. Kopeyan, H. Schweitz, M. Lazdunski, Structure–function relationship in the binding of snake neurotoxins to the Torpedo membrane receptor, Biochemistry 14 (1975) 2081–2091.